

## Letter

Abdel El Fatimy\*, Anindya Nath, Byoung Don Kong, Anthony K. Boyd, Rachael L. Myers-Ward, Kevin M. Daniels, M. Mehdi Jadidi, Thomas E. Murphy, D. Kurt Gaskill and Paola Barbara\*

# Ultra-broadband photodetectors based on epitaxial graphene quantum dots

<https://doi.org/10.1515/nanoph-2017-0100>

Received October 8, 2017; revised November 28, 2017; accepted December 7, 2017

**Abstract:** Graphene is an ideal material for hot-electron bolometers due to its low heat capacity and weak electron-phonon coupling. Nanostructuring graphene with quantum-dot constrictions yields detectors of electromagnetic radiation with extraordinarily high intrinsic responsivity, higher than  $1 \times 10^9 \text{ V W}^{-1}$  at 3 K. The sensing mechanism is bolometric in nature: the quantum confinement gap causes a strong dependence of the electrical resistance on the electron temperature. Here, we show that this quantum confinement gap does not impose a limitation on the photon energy for light detection and these quantum-dot bolometers work in a very broad spectral range, from terahertz through telecom to ultraviolet radiation, with responsivity independent of wavelength. We also measure the power dependence of the response. Although the responsivity decreases with increasing power, it stays higher than  $1 \times 10^8 \text{ V W}^{-1}$  in a wide range of absorbed power, from 1 pW to 0.4 nW.

**Keywords:** graphene; hot-electron bolometers; quantum dots.

\*Corresponding authors: Abdel El Fatimy and Paola Barbara,

Department of Physics, Georgetown University, Washington, DC 20057, USA, e-mail: a.elfatimy@gmail.com (A. El Fatimy); paola.barbara@georgetown.edu.

<http://orcid.org/0000-0003-4151-262X> (P. Barbara)

Anindya Nath, Byoung Don Kong, Anthony K. Boyd, Rachael L. Myers-Ward, Kevin M. Daniels and D. Kurt Gaskill: U.S. Naval Research Laboratory, Washington, DC 20375, USA

M. Mehdi Jadidi and Thomas E. Murphy: Institute for Research in Electronics and Applied Physics, University of Maryland, College Park, MD 20742, USA

## 1 Introduction

Graphene is a broadband light absorber because it is a gapless material [1, 2]. At low frequencies, up to the terahertz range, light absorption mainly occurs via intraband transition and it is determined by the graphene Drude conductivity [3, 4]. At frequencies above the infrared range, interband optical transitions dominate, and light absorption reduces to a constant value, about 2.3% per graphene layer [4, 5]. In all cases, electrons thermalize via electron-electron interactions within a timescale of tens of femtoseconds [6–8] and via emission of optical phonons within a few hundreds of femtoseconds [9, 10]. After thermalization, the effective electron temperature  $T_e$  can be higher than the temperature of the graphene lattice, of the substrate, and of the metal contacts attached to the graphene due to the small electronic heat capacity and the ineffective cooling from collisions with acoustic phonons [11, 12].

Similar to other materials where hot-charge carriers have been exploited in the design of optoelectronic devices [13, 14], there have been several demonstrations of hot-electron graphene detectors. Photothermal effect detectors use an asymmetric device architecture (PN junctions [15, 16] or contacts made of different materials [17]) to produce a net current of hot electrons. For symmetric graphene devices, the increase in electron temperature can be measured either via Johnson noise thermometry [18, 19] or using the variation of the graphene resistance as a function of temperature [20–22]. In this latter case, the detector performance directly depends on how strongly the graphene resistance varies as a function of temperature. One important figure of merit is the bolometer responsivity, which is defined as the change of voltage  $\Delta V_{DC}$  across the device caused by the incident light divided by the absorbed power,  $r = \Delta V_{DC} / \Delta P = I_{DC} (\Delta R / \Delta P) = (I_{DC} / G_{TH}) (\Delta R / \Delta T)$ , where  $G_{TH}$  is the thermal conductance,  $\Delta R$  is the change in resistance caused by a temperature increase  $\Delta T$ , and  $\Delta V_{DC}$  is measured at a constant current  $I_{DC}$ .

We recently showed that nanostructured quantum-dot constrictions in epitaxial graphene grown on SiC yield terahertz detectors with extraordinarily high responsivity [23]. The detection of 2-mm-wavelength (150 GHz) radiation from quantum dots with different dot diameters revealed that the quantum confinement gap in the dot causes a strong temperature dependence of the graphene electrical resistance and therefore a high responsivity. The quantum confinement gap is a combination of the charging energy of the dot and the electronic level spacing, and it produces a potential barrier to the current flowing through the graphene [24–27]. The barrier heights extracted from fits of the temperature dependence of the resistance to a thermal activation behavior ranged from 0.5 to 4 meV for dot diameters varying from 200 to 30 nm. In all cases, the barrier height was larger than (or, for the largest dots, comparable to) the photon energy at 150 GHz (about 0.6 meV), leaving it unclear whether the quantum-dot bolometers would operate at frequencies with photon energy higher than the barrier height and whether the performance would be frequency dependent. In this work, we study light detection from these graphene quantum dots up to photon energies a thousand times larger than the thermal activation barrier and show that the responsivity is completely independent of frequency. This can be explained by considering both charge carrier dynamics in graphene and quantum transport through the quantum dot. We also characterize the response as a function of absorbed power and find a sublinear dependence of the photovoltage on absorbed power, leading to a decrease of responsivity with absorbed power. The quantum-dot devices nonetheless show responsivity higher than  $1 \times 10^8$  V W<sup>-1</sup>, at least three orders of magnitudes higher than the highest responsivity reported for other types of graphene bolometers [20–22], over a wide range of absorbed power, from 1 pW to 0.4 nW.

## 2 Results and discussion

The quantum dots were fabricated using e-beam lithography on epitaxial graphene grown on SiC and following the fabrication procedure described in Refs. [23, 28]. The samples were mounted on a gold plate and placed in a cryostat behind a picarin vacuum window. Filters were inserted to control the optical input power and restrict the wavelength to eliminate thermal blackbody radiation.

Figure 1A shows the temperature dependence of the electrical resistance  $R(T)$  of a 100-nm-diameter quantum

dot (red curve). In our previous work [23], we characterized the performance of the graphene quantum-dot bolometers as a function of temperature and dot diameter and showed that the smallest dots (with a diameter smaller than 100 nm) yield the best performance (responsivities higher than  $1 \times 10^{10}$  V W<sup>-1</sup>) because they have the largest quantum confinement gap and the strongest variation of resistance with temperature. In this work, we focus on the study of the bolometer performance as a function of radiation wavelength and absorbed power, using dots of intermediate size, with diameters ranging from 100 to 200 nm. All the measurements presented here are performed at the base lattice temperature  $T_0 = 3$  K. The dependence of the device performance on the base lattice temperature can be found in Ref. [23].

Figure 1D shows the photoresponse of a 200 nm dot. The black curve is the current-voltage (IV) characteristic of the dot with radiation OFF. The curve tends to be nonlinear due to Joule heating: when the bias and the Joule power increase, the resistance decreases, as can be seen in Figure 2A (inset). This qualitative behavior occurs in all the dots; however, the IV curves are very sensitive to the dot diameter and the orientation of the graphene bolometer with respect to the steps between the crystal planes on the surface of the SiC substrate, as these two factors affect the temperature dependence of the bolometer resistance [23]. As a result, the IV curves of devices designed with the same dot diameter such as those in Figures 1D and 2A show some differences due to variations in the actual dot diameter after the fabrication process and in their orientation with respect to the steps on the substrate [23].

Under illumination, the resistance decreases further. The red, green, and purple curves in Figure 1B show the IV characteristics when the sample is irradiated with light at three different wavelengths ranging from millimeter-wave to ultraviolet (2, 1543, and 365 nm, respectively). The sample clearly shows a response in this wide range of wavelengths. We analyze the response by measuring the power absorbed by our devices from the IV curves. Figure 2A shows the response of a device as a function of power for illumination at 2 mm wavelength (0.15 THz). For every value of incident power, we measure the power absorbed by the bolometer with the same method that we used in Ref. [23].

We first measure the differential resistance at zero bias for the IV characteristic with radiation ON and then find the point in the IV characteristic with radiation OFF that exhibits the same differential resistance. We use the Joule power dissipated in the bolometer at that point,  $P = I_{\text{DC}} V_{\text{DC}}$ , as a measurement of the radiation power absorbed when

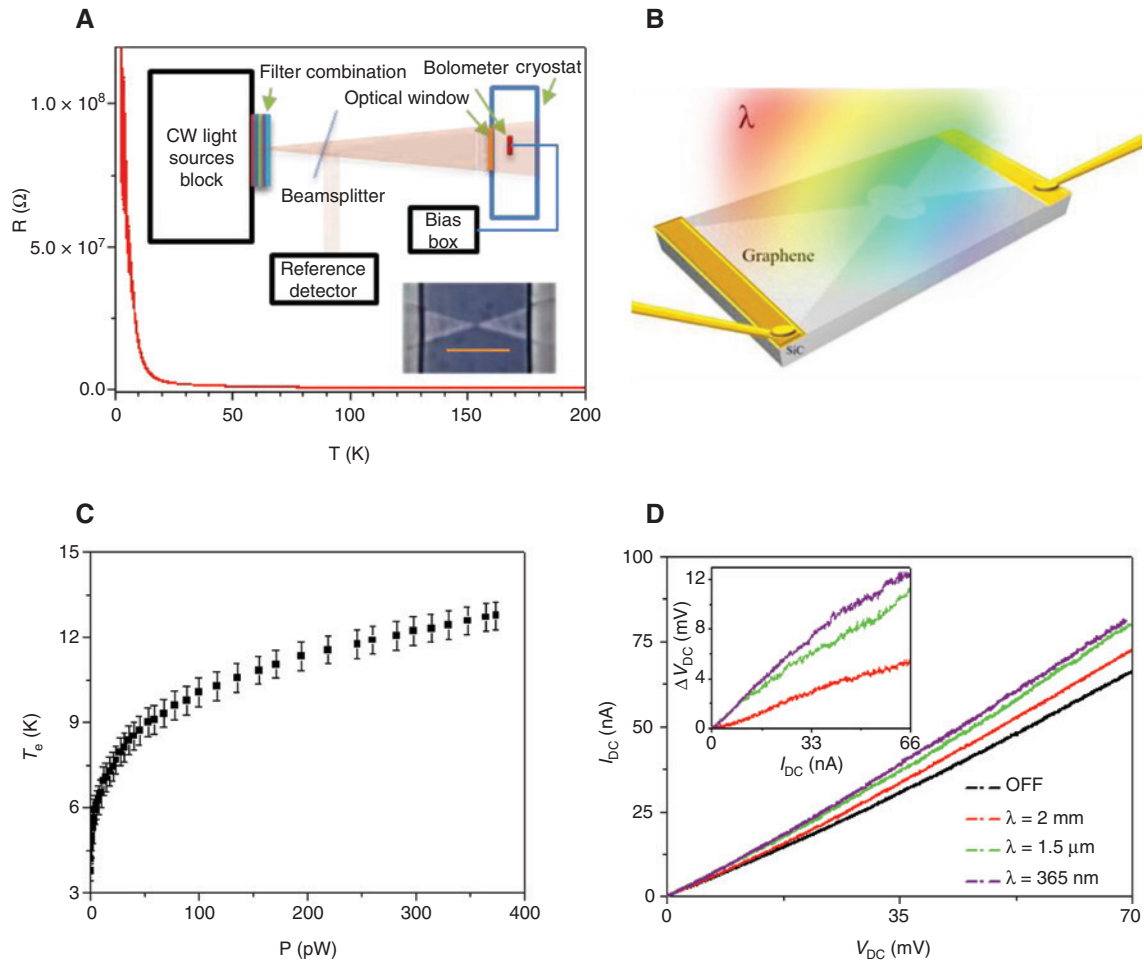


**Figure 1:** Ultra-broadband bolometric response.

(A) Resistance as a function of temperature for a quantum dot with a diameter of 100 nm. Inset: schematic of the experimental setup and optical image of a typical quantum dot. Scale bar,  $3 \mu\text{m}$ . (B) Sketch of a typical device with broadband radiation. (C) Electron temperature as a function of joule power for a quantum dot with a diameter of 200 nm. (D) IV characteristic of a 200 nm dot without radiation (OFF, black) and with radiation at 2 mm (red), 1.543 mm (green), and 365 nm (purple) wavelength, having absorbed power of 0.4, 1.0, and 1.4 nW, respectively. Inset: response  $\Delta V_{DC}$  as a function of the current  $I_{DC}$  at the same wavelengths.

the light is ON. We repeat the same procedure for every IV curve that we obtain when varying the power of the incident light.

The photovoltage  $\Delta V_{DC}$  at a fixed current,  $I_{DC} = 1.9$  nA, for different values of the absorbed power is shown in Figure 2B (black squares). The sublinear dependence of  $\Delta V_{DC}(P)$  is expected because the variation of resistance versus temperature is highest at low temperature (see Figure 1A) and becomes weaker when the electron temperature increases due to an increase in the absorbed power. As  $\Delta V_{DC}$  is sublinear as a function of absorbed power, the responsivity decreases with increasing radiation power, but it is still very high for a large range of absorbed power, as shown in Figure 2B (inset), where we include data from six devices, including two small-diameter devices with 30 nm dots.

The responsivity is larger for dots of smaller diameter. Figure 3 shows the power dependence of the responsivity for a 100-nm-diameter dot. Measurements at the lowest values of absorbed power in Figure 3A show that absorbed power below 1 pW can be detected at all the measured wavelengths by measuring changes in  $V_{DC}$ . Higher sensitivity can be achieved with temporally modulated illumination using lock-in detection.

In all the measurements above, we have reported the absorbed power. Although this gives the ultimate performance of the devices, it is most useful to characterize their performance in terms of incident power. The optical coupling efficiency (the ratio between absorbed power and incident power) varies with radiation wavelength. For our long-wavelength source (2 mm, where the absorption is dominated by the graphene Drude conductivity),

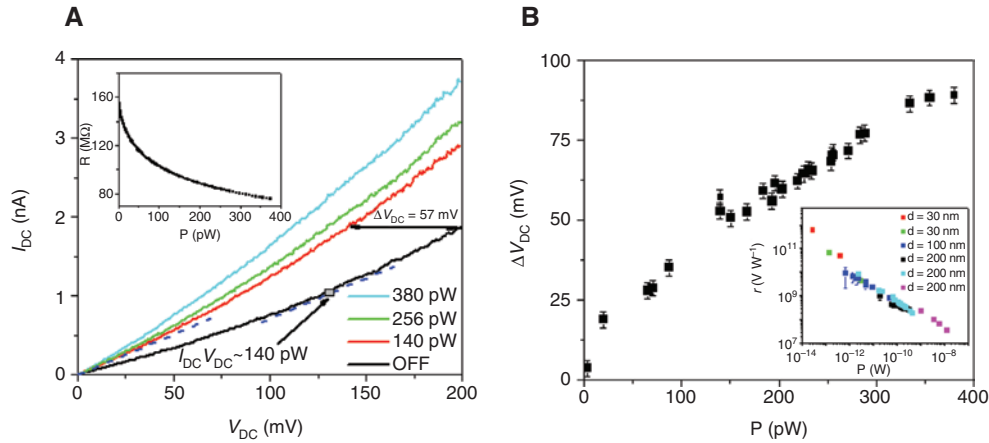


**Figure 2:** Measurements of photovoltage and absorbed power from IV curves.

(A) IV characteristic of a 200 nm dot without radiation (black) and with 2-mm-wavelength radiation (colors) at different values of absorbed power. Dashed lines indicate points in the curves with the same differential resistance. Inset: differential resistance of the curve with radiation OFF at different values of Joule power. (B) Photovoltage measured from the device in (A) at  $I_{DC} = 1.9$  nA as a function of absorbed power under illumination with a 2-mm-wavelength source (black squares). Inset: responsivity vs. absorbed power for the same device (black squares) and five other devices. The legend indicates the diameter of the quantum dot for each device.

it can be optimized by designing antennas that are either broadband or tuned at specific wavelengths [29]. For wavelengths of 1500 nm or shorter, the coupling efficiency is limited by the optical absorption of a single graphene layer (2.3%). Our measured ratio of absorbed to incident power at 1543 nm is a bit higher (2.7%; see Methods) and it is possibly enhanced by the reflection of radiation from the gold plate under the bottom surface of the SiC substrate. Optical cavities can be also used to enhance the detector absorption [30].

We use the measured responsivity at different wavelengths to calculate the total electrical noise equivalent power (NEP) for the bolometers, including contributions

from Johnson noise, shot noise, and thermal fluctuations [31] ( $NEP^2 = NEP_{JN}^2 + NEP_{SN}^2 + NEP_{TF}^2 = (4k_B TR)/r^2 + (2eI_{DC})R^2/r^2 + 4k_B T^2 G_{TH}$ , where  $G_{TH}$  is extracted from the data using the IV and  $R(T)$  curves [23]). Figure 3 indicates that the responsivity and the NEP are independent of radiation wavelength for photon energies in a very wide range of the radiation spectrum, including photon energies that are orders of magnitude larger than the activation energy of the dot. These behaviors can be explained by considering charge carrier dynamics after light absorption. As mentioned earlier, the timescale for electrons to equilibrate at an effective electron temperature via electron-electron collisions and optical phonon emission is on the order of

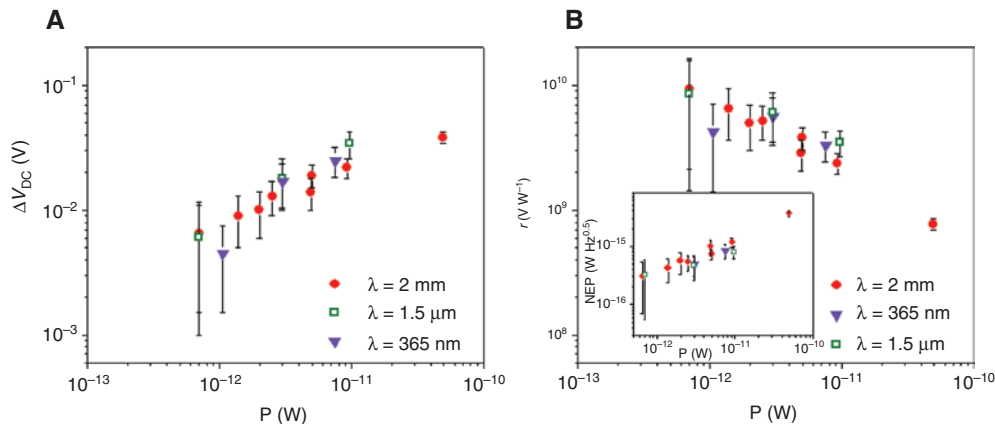


**Figure 3:** Power dependence of the response.

(A) Low power dependence of the response from a 100 nm dot under illumination at different wavelengths. (B) Responsivity as a function of absorbed power at different wavelengths. Inset: calculated electrical NEP as a function of absorbed power at various wavelengths.

10–100 fs. This timescale is extremely fast compared to the charging time of the dot. We can estimate the capacitance of the dot by considering that the charging energy must be larger than the activation energy of the dot. This is because the activation energy depends on the alignment of the Fermi energy of the source and drain electrodes within the quantum confinement gap (it can be tuned to zero by doping the dot and aligning the Fermi energy to the top of the quantum confinement gap). The capacitance corresponding to a charging energy of 10 meV is about 10 aF, giving an RC time of 1 ns for a dot resistance of 100 M $\Omega$ . As electrons equilibrate with a much faster timescale, the photon energy and the specific wavelength do not play any role in the quantum transport of charges through the dot. As a result, we find that the absorbed power (regardless of wavelength) and the corresponding electron temperature are the only factors that determine the current through the dot.

### 3 Conclusions

In conclusion, the bolometric detectors show excellent electrical responsivity, higher than  $10^9$  V W<sup>-1</sup>, which is independent of frequency over an ultra-broadband spectrum, from subterahertz to ultraviolet. Even with larger (100 nm) dots, incident power as low as 30 pW at 1543 nm is easily detected by directly measuring the photovoltage  $\Delta V_{DC}$ . Although the responsivity decreases with increasing power, it is still at least three orders of magnitudes higher than other types of graphene bolometers and it can be further optimized using lock-in detection techniques. Future work will focus on pushing the performance limits of the device using smaller quantum dots and on optimizing the coupling of the incident radiation to the bolometer by designing optical cavities and antennas.

### 4 Methods

We used three light sources: a backward wave oscillator (Microtech) for the 2-mm-wavelength radiation, a 1543 nm 81663A DFB laser source (Agilent), and a 365 nm LED UV source (U-Vix). The coupling efficiency for the 1543-nm-wavelength source was estimated from the ratio of the absorbed power to the incident power. The incident power was estimated by multiplying the incident power density by the area of the graphene (20  $\mu\text{m}^2$ , including the dot and the two triangular regions attached to it). The incident power density was measured with a calibrated detector

81524A InGaAs optical head with 8153A lightwave multi-meter (HP).

**Acknowledgments:** This work was supported by the U.S. Office of Naval Research (award nos. N00014-13-1-0865 and N00014-16-1-2674 to Georgetown University and the University of Maryland as well as support to the U.S. Naval Research Laboratory) and the NSF (ECCS 1610953). This research was performed while Kevin M. Daniels held an NRC Research Associateship award at the U.S. Naval Research Laboratory.

### References

- [1] Geim AK, Novoselov KS. The rise of graphene. *Nat Mater* 2007;6:183–91.
- [2] Castro Neto AH, Guinea F, Peres NMR, Novoselov KS, Geim AK. The electronic properties of graphene. *Rev Mod Phys* 2009;81:109–62.
- [3] Dawlaty JM, Shivaraman S, Strait J, et al. Measurement of the optical absorption spectra of epitaxial graphene from terahertz to visible. *Appl Phys Lett* 2008;93:131905–7.
- [4] Sensale-Rodriguez B, Yan RS, Liu L, Jena D, Xing HG. Graphene for reconfigurable terahertz optoelectronics. *Proc IEEE* 2013;101:1705–16.
- [5] Nair RR, Blake P, Grigorenko AN, et al. Fine structure constant defines visual transparency of graphene. *Science* 2008;320:1308–8.
- [6] Breusing M, Kuehn S, Winzer T, et al. Ultrafast nonequilibrium carrier dynamics in a single graphene layer. *Phys Rev B* 2011;83:153410–13.
- [7] Tielrooij KJ, Song JCW, Jensen SA, et al. Photoexcitation cascade and multiple hot-carrier generation in graphene. *Nat Phys* 2013;9:248–52.
- [8] Brida D, Tomadin A, Manzoni C, et al. Ultrafast collinear scattering and carrier multiplication in graphene. *Nat Commun* 2013;4:1987–95.
- [9] Sun D, Wu ZK, Divin C, et al. Ultrafast relaxation of excited dirac fermions in epitaxial graphene using optical differential transmission spectroscopy. *Phys Rev Lett* 2008;101:157402–6.
- [10] Wang HN, Strait JH, George PA, et al. Ultrafast relaxation dynamics of hot optical phonons in graphene. *Appl Phys Lett* 2010;96:081917–20.
- [11] Song JCW, Rudner MS, Marcus CM, Levitov LS. Hot carrier transport and photocurrent response in graphene. *Nano Lett* 2011;11:4688–92.
- [12] Betz AC, Violla F, Brunel D, et al. Hot electron cooling by acoustic phonons in graphene. *Phys Rev Lett* 2012;109:056805–9.
- [13] Tam S, Hu CM. Hot-electron-induced photon and photocarrier generation in silicon MOSFETs. *IEEE Trans Electron Devices* 1984;31:1264–73.
- [14] Xu KK. Integrated silicon directly modulated light source using p-well in standard CMOS technology. *IEEE Sensors J* 2016;16:6184–91.
- [15] Gabor NM, Song JCW, Ma Q, et al. Hot carrier-assisted intrinsic photoresponse in graphene. *Science* 2011;334:648–52.

- [16] Graham MW, Shi SF, Ralph DC, Park J, McEuen PL. Photocurrent measurements of supercollision cooling in graphene. *Nat Phys* 2013;9:103–8.
- [17] Cai X, Sushkov AB, Suess RJ, et al. Sensitive room-temperature terahertz detection via the photothermoelectric effect in graphene. *Nat Nanotechnol* 2014;9:814–9.
- [18] McKitterick CB, Prober DE, Vora H, Du X. Ultrasensitive graphene far-infrared power detectors. *J Phys Condensed Matter* 2015;27:164203–15.
- [19] Betz AC, Jhang SH, Pallecchi E, et al. Supercollision cooling in undoped graphene. *Nat Phys* 2013;9:109–12.
- [20] Yan J, Kim MH, Elle JA, et al. Dual-gated bilayer graphene hot-electron bolometer. *Nat Nanotechnol* 2012;7:472–8.
- [21] Han Q, Gao T, Zhang R, et al. Highly sensitive hot electron bolometer based on disordered graphene. *Sci Rep* 2013;3:3533–8.
- [22] Vora H, Kumaravadivel P, Nielsen B, Du X. Bolometric response in graphene based superconducting tunnel junctions. *Appl Phys Lett* 2012;100:153507–11.
- [23] El Fatimy A, Myers-Ward RL, Boyd AK, Daniels KM, Gaskill DK, Barbara P. Epitaxial graphene quantum dots for high-performance terahertz bolometers. *Nat Nanotechnol* 2016;11:335.
- [24] Ponomarenko LA, Schedin F, Katsnelson MI, et al. Chaotic dirac billiard in graphene quantum dots. *Science* 2008;320:356–8.
- [25] Guttinger J, Molitor F, Stampfer C, et al. Transport through graphene quantum dots. *Rep Prog Phys* 2012;75:126502–25.
- [26] Stampfer C, Guttinger J, Hellmueller S, Molitor F, Ensslin K, Ihn T. Energy gaps in etched graphene nanoribbons. *Phys Rev Lett* 2009;102.
- [27] Droescher S, Knowles H, Meir Y, Ensslin K, Ihn T. Coulomb gap in graphene nanoribbons. *Phys Rev B* 2011;84:073405–10.
- [28] Yang YF, Huang LI, Fukuyama Y, et al. Low carrier density epitaxial graphene devices on SiC. *Small* 2015;11:90–5.
- [29] Rinzan M, Jenkins G, Drew HD, Shafranuk S, Barbara P. Carbon Nanotube quantum dots as highly sensitive terahertz-cooled spectrometers. *Nano Lett* 2012;12:3097–100.
- [30] Heath RM, Tanner MG, Kirkwood RA, Miki S, Warburton RJ, Hadfield RH. A tunable fiber-coupled optical cavity for agile enhancement of detector absorption. *J Appl Phys* 2016;120:113101–9.
- [31] Richards PL. Bolometers for infrared and millimeter waves. *J Appl Phys* 1994;76:1–24.